Int J Adv Manuf Technol
DOI 10.1007/s00170-015-7566-4

ORIGINAL ARTICLE

Mold structure design and casting simulation of the high-pressure die casting for aluminum automotive clutch housing manufacturing

Seong Il Jeong[1] · Chul Kyu Jin[1] · Hyung Yoon Seo[2] · Jong Deok Kim[2] · Chung Gil Kang[3]

Received: 23 February 2015 / Accepted: 5 July 2015

Abstract This study aims at a mold design based on the casting simulation and mold structural simulation in order to manufacture automotive clutch housing aluminum parts in a high-pressure die casting process. For melt to flow into the mold and fill to the product section evenly, a gating system with five gates was designed. MAGMAsoft, a casting simulation program, was used to predict or prevent the possibility of casting defects that may occur in the filling process and solidification process. The way to select proper casting devices for the clutch housing product is also presented. A structural simulation of the mold base was conducted by means of ANSYS Workbench to predict possible damage to the vulnerable part of the mold right from the step of mold design. In the actual shot test, five clutch housing products in total were manufactured. All of them were fully filled and involved no defect on the surface. The spot of shrinkage porosity predicted in the casting simulation and the spot of actual occurrence were not exactly the same but quite close. The degree of hardness of these products was about 84 HV regardless of location.

Keywords High-pressure die casting · Mold structure · Casting simulation · Casting defects · Aluminum alloy

✉ Chung Gil Kang
cgkang@pusan.ac.kr

[1] Graduate School of Mechanical and Precision Engineering, Pusan National University, San 30 Chang Jun-dong, Geum Jung-Gu, Busan 609-735, South Korea

[2] Department of Computer Science and Engineering, Pusan National University, San 30 Chang Jun-dong, Geum Jung-Gu, Busan 609-735, South Korea

[3] School of Mechanical Engineering, Pusan National University,, San 30 Chang Jun-dong, Geum Jung-Gu, Busan 609-735, South Korea

1 Introduction

Die casting began when Doehle manufactured die casting products by using aluminum alloys in 1915, and since then, the demands have gradually increased as the automotive industry developed [1]. Among casting methods of aluminum automotive parts, the most commonly used ones are divided to low-pressure die casting, gravity die casting, and high-pressure die casting. The low-pressure casting and gravity casting are applicable to automotive parts difficult to make such as cylinder head because the internal structure is formed in one mold. Recently, many of automotive parts that have been produced usually in such ways as low-pressure casting and gravity casting started to be light-weighted in application of high-pressure die casting for mass production through one single mold [2–7]. High-pressure die casting (HPDC) is advantageous in that it can mass-produce complicated and precise shapes within a short time from tens of seconds or 100~180 s.

In the past, die casting mold design was challenging as the trial and error method was applied by mold designers and on-site technicians. The mold design process of high-pressure die casting, in contrast, adopts computer-aided engineering (CAE), includes the filling and solidification processes in the early development stage to predict and evaluate the quality, and thus establishes the optimal way of mold design [5, 8–10]. Today, a number of designers adopt mold design methods that combine CAE and their practical experiences, which reduces fraction defective, saves costs, and shortens the development period. In addition, since it is possible to predict mold sticking and deformation, this method is of great help when it comes to structural design of molds.

This study includes a casting simulation for clutch housing products that control or deliver the dynamic force of an automotive engine using MAGMA. Predicted or prevented are

Published online: 19 September 2015

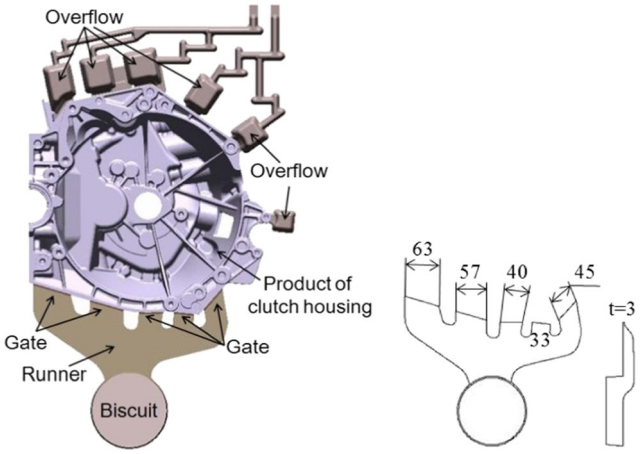

Fig. 1 Gating system design of clutch housing

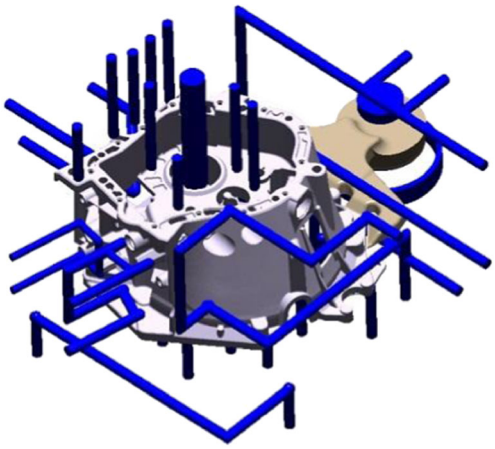

Fig. 3 Cooling line of mold

casting defects possible in the filling and solidification process of a casting simulation. Efforts were also put forth into minimizing casting expenses. The gating system design and product shape were applied to mold design with the aim to produce optimized quality products with minimal casting defects. For casting equipment selection and structural simulation of the mold base, ANSYS Workbench was utilized to predict mold damages to the vulnerable section of a mold right from the step of mold design, save mold production costs through the optimal mold design, and to reduce other mold modifications and expenses that might additionally occur by minimizing times of experiments.

2 Conditions of simulation and experiment

2.1 Mold modeling

Solid modeling for clutch housing products was conducted by means of Pro/ENGINEER, a commercial 3D modeling program, and then other sections such as biscuit, runner, gate, and overflow were also modeled in the order. Figure 1 shows an example of mold modeling to manufacturer clutch housing parts in application of the high-pressure die casting method. Five gates were used, and the thickness was 3 mm.

Figure 2 shows the 3D image of a mold in actual size modeled by using Pro/ENGINEER. The total weight of the mold weighed in 3D modeling was about 12.52 ton, the fixed mold about 3.83 ton, and the moving mold about 8.69 ton, respectively. Two slide cores were operated with five tunnel pins. Specially applied was a chill block with no vacuum device. To prevent dispersion toward the chill block upon casting, a vent insert was added between the moving core and chill block as a shock-observing device to decelerate melting. A slipper was added around the four guide pins to handle problems that might occur to the mold. To prevent the slide core from being pushed toward the hydraulic cylinder upon closing the mold, a retrograding-preventive plate was installed on the fixed mold base. A distributor in contact with the sleeve was designed in a plate type. The hydraulic cylinder applied to

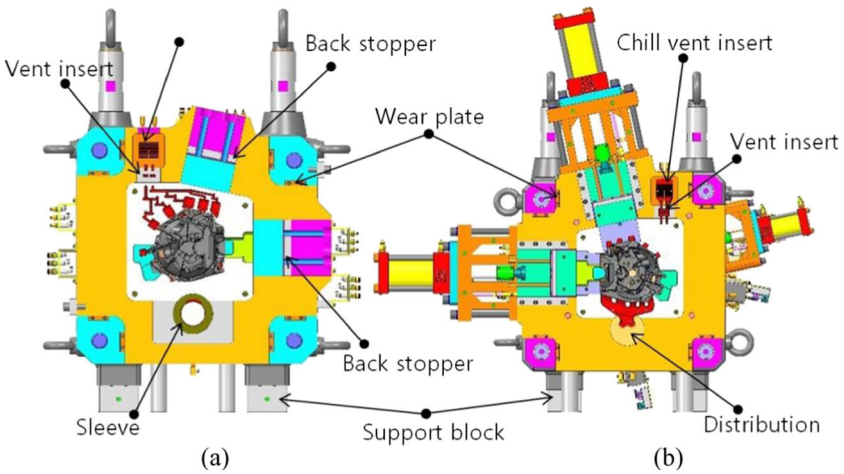

Fig. 2 3D mold modeling: **a** fixed mold and **b** movable mold

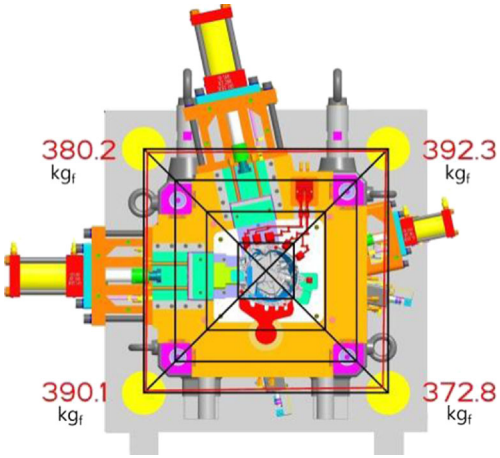

Fig. 4 Locking force in each quadrant of movable mold

the slide was of a diode FA type. A rectangular thin hydraulic cylinder was applied to tunnel pins. The limit switches were of lever and push types, rather than those for proximity sensors, for the operator's safety. As for the ejector of die casting, the ejector bar is connected directly to the plate instead of using a C-plate clamp. Figure 3 shows the cooling channel installed for the mold. Spot cooling and line cooling methods were mixed around the mold.

2.2 Selection of casting devices

For casting device selection, the working force was calculated based on Eq. (1) below, which indicates the relation between the projected area of casting and casting pressure applied to the mold. In fact, however, the mold clamping force actually necessary could be larger than the force applied to the mold, and thus the mold clamping force was calculated by using Eq. (2) [11]

$$F_s = P_m \times A_p \quad (1)$$

where F_s indicates the working force applied to the mold, P_m is the casting pressure, and A_p is the general area of projection

$$T = \left(P_m \times A_p \times C\right)/1000 \quad (2)$$

where T indicates the actual mold clamping force and C is the safety coefficient.

For Al alloy die casting, the mechanical properties would improve drastically up to 49 MPa of casting pressure, but over 78.45 MPa, the porosity removing effect is insignificant.

Table 1 Chemical composition of GCD500 (wt%)

C	Si	Mn	P	S	Mg	Fe
≥2.5	≤2.7	≤0.4	≤0.08	≤0.02	≤0.09	bal

Table 2 Mechanical properties of GCD500

Tensile strength	Yield strength	Elongation	Hardness
≥500 MPa	≥320 MPa	≥7 %	150~230 HB

Thus, the casting pressure is set to 49~78 MPa in general [12]. In consideration of the shocking force of a plunger, it is appropriate to select a die casting device with mold clamping force 20~25 % greater than the working force (F_s). When the safety rate to the mold clamping force of a 1600-ton casting device is 20 %, the general area of projection of the clutch housing is 1706.4 cm^2. When the casting pressure is 78.4 MPa, the mold clamping force is 1638.1 ton, which exceeds 1600 ton of the applied equipment. Thus, the casting pressure was decreased down to 73.5 MPa, and the mold clamping force was 1535.4 ton (safety rate 20 %) for the die casting process. The force in each quadrant applied to each tie bar of the casting equipment was calculated on the assumption that the safety rate of the mold clamping force would be 20 %. Figure 4 shows the mold clamping force applied to a quadrant of the mold. The force in each quadrant applied to each tie bar was even as high as 392~372 kg_f.

2.3 Structural simulation of a mold base

To confirm the safety of the mold structure, a structural simulation was conducted by means of ANSYS Workbench. The analysis of mold base deformation at the moving section was followed by the assessment of structural safety.

The chemical composition and mechanical properties of ductile iron (GCD500) for the mold base are presented in Table 1 and Table 2, respectively. Table 3 and Fig. 5 show mold structure information and Young's modulus and Poisson's ratio of ductile iron in reflection of the mold design for structural simulation.

To calculate the secure thickness of the mold base, the basic thickness was determined in application of the simplified calculation expression. After the safety coefficient 1.5 was applied to the result of the calculation,

Table 3 Conditions for structure analysis of movable mold base

Classification	Conditions		Classification	Conditions
Cast area (A)	1197.56 cm^2		Mold width (b)	113 cm
Die base legs distance (l)	57 cm		Cast pressure (P)	73.54 MPa
Mold base thickness (h)	1st	18 cm	Young's modulus	150×10^9 N/m^2
	2nd	20 cm		
	3rd	22 cm	Poisson's ratio	0.28
	4th	24 cm		

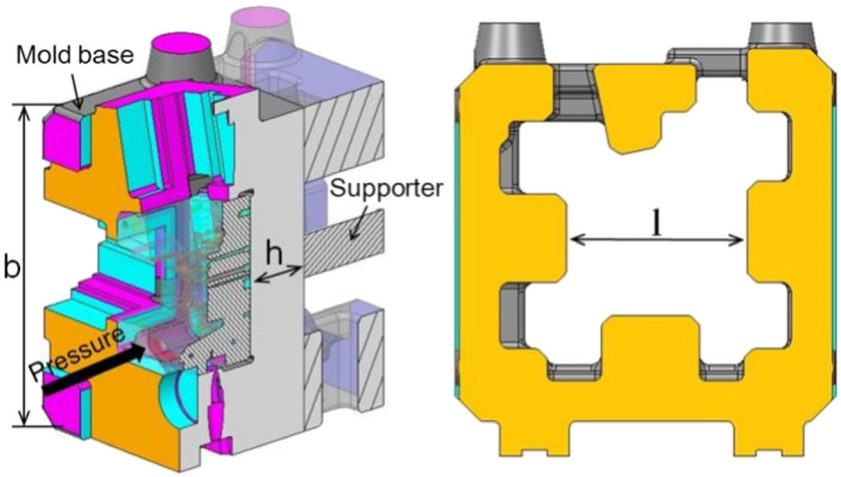

Fig. 5 Shape condition of movable mold base for structural analysis

deformation as much as 0.2~0.25 mm was applied to the design. This data was reanalyzed to the structural simulation in the most realistic conditions by using ANSYS Workbench. When the max. deformation value was 0.23 mm or higher in the structural simulation, it was judged as "fail," and then a reanalysis was conducted by changing the value from the first to the second. When the max. deformation was lower than 0.23 mm, the thickness was reset to optimize the design and then a structural simulation was conducted again.

To simplify the hardness calculation process, applied was Eq. (3) below on the max. deflection (δ_{max}) of the simple beam's distributed load:

$$\delta_{max} = 5WL^4/384EI \tag{3}$$

Table 4 Conditions of high-pressure die casting

	Classification	Conditions	Initial temperature
Material	Cast	ALDC12	650 °C
	Fixed die	STD 61	250 °C
	Moving die	STD 61	
	Cooling material	Water	30 °C
Machine	Machine type	1600 ton	–
	Tip diameter	Φ120 mm	
	Active length of shot sleeve	860 mm	
	Filled rate of sleeve	40.47 %	
Cast conditions	Cast pressure	73.5 MPa	–
	Slow shot velocity	0.3 m/s	
	Fast shot velocity	3.0 m/s	
	Length of slow-speed region	625 mm	
	Length of fast speed region	235 mm	

where W indicates the evenly distributed load, L is the simple beam distance, E is Young's modulus, and I is the section's second moment.

2.4 Casting simulation conditions

The governing equation used for the filling and solidifying analysis of MAGMAsoft is on the assumption that fluid flows and heat transfer are according to mass conservation law, momentum conservation law, and energy conservation law.

The MAGMA soft package used in this study has the following characteristics [5]:

(1) Ease of physical interpretation of various steps of algorithms
(2) Conservation of physical properties
(3) Better convergence than pure finite element or finite difference methods (FEM or FDM)
(4) Reduction of solution time

Governing equations used for fluid and solidification analyses of 3D incompressible flows include continuity equation, Navier-Stokes equation, energy equation, and volume of fluid. Filling analysis involves finite differential method (FDM) [5]. For the accuracy and casting analysis time minimization in a casting simulation, a manual element dividing method was adopted for Mesh Generation with 37,000,000 volumes as the goal. Mesh for Solver5, applicable to thin-walled projects, was used. The number of divided metal cells (except for

Table 5 Chemical composition of ALDC12 alloy (wt%)

Si	Cu	Mg	Mn	Zn	Ni	Sn	Fe	Al
9.6~11.5	2~3	≤0.1	≤0.5	≤3.0	≤0.3	≤0.2	≤1.3	bal

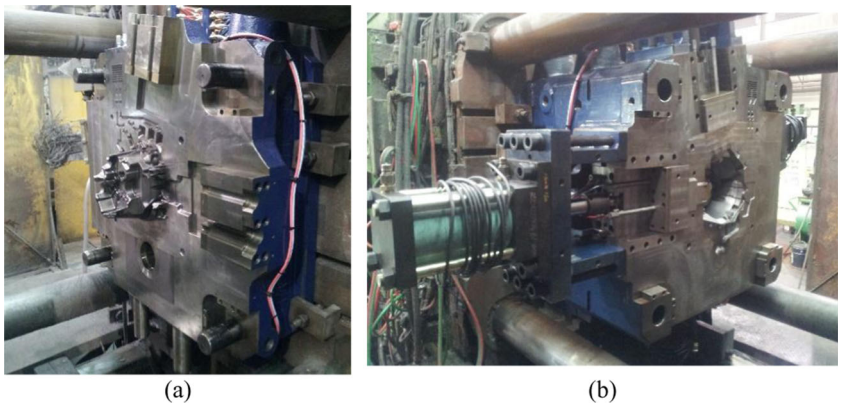

(a) (b)

Fig. 6 Molds assembled high-pressure die casting machine: **a** fixed mold and **b** movable mold

molds) was 988,817, and the number of elements was 37,160, 832 volumes total in the casting simulation.

The casting simulation conditions are presented in Table 4. The pouring temperature is 650 °C, and all mold materials were STD 61. As for the heat transfer definitions between material groups of MAGMAsoft, temperature-dependent HTC value of MAGMAsoft was applied to the cast and mold. The value between mold and mold was 3500 W/m^2 K and that of between mold and cooling channel was 7000 W/m^2 K.

In this casting simulation, even mold erosion and die sticking that might occur in an actual shot test were predicted through the analysis. To obtain casting simulation results similar to those in actual on-site conditions, the initial temperature of mold parts was set to 25 °C, and the number of cycles in which mold temperature started to be stabilized with no pre-heating applied was checked. As a result, it turned out that mold temperature was stabilized in the seventh cycle, which was applied to the actual shot test.

De casting device applied to the casting simulation is the 1600-ton cold chamber die casting machine. The plunger tip ∅120 mm and the shot sleeve's length 860 mm. The working pressure was set to 73.5 MPa to prevent it from exceeding the device capacity. As for the plunger tip, the speed remained at 0.3 m/s in the low-speed area up to 625 mm, and from then on, the filling was conducted at the speed of 3.0 m/s. To enhance the quality, the chill vent was applied instead of the gas vent. ALDC 12 die casting aluminum alloy was used in the simulation and experiment process. Table 5 shows the chemical composition of ALDC 12.

Table 6 Simple calculations and structural analysis comparing the results

Mold base thickness, h (cm)		Simple calculation value (mm)	Structural analysis results (mm)	
			Supporter unapplied (max)	Supporter applied (max)
1st	18	0.387	–	–
2nd	20	0.282	0.2371	0.2178
3rd	22	0.212	0.2334	0.2159
4th	24	0.164	0.2248	0.2115
Final	23	0.186	0.2279	0.2131

2.5 Shot test conditions

Figure 6 shows the fixed and moving sections of the mold installed at the 1600-ton die casting. The injection conditions are the same as in the casting simulation of MAGMA presented in Table 4. For 3 to 5 min before the injection, the mold surface was pre-heated by means of a torch. This was repeated five to six times at low speed of 0.3 m/s in the first pre-heating work and then three more times at high speed of 3.0 m/s in the second pre-heating work. After five injections in total, five clutch housing parts were produced. After casting, the products were pulled out of the mold and went through the quenching process in water.

The microstructure and Vickers hardness of the produced clutch housing parts were measured. The microstructure was measured at the thickest part and average-thick part. Vickers hardness was measured five times at each location with the fitting load set to 200 g.

3 Results and discussion

3.1 Structure simulation of mold base

Table 6 presents the structural simulation results and calculation of simplified Eq. (3). To calculate max. deflection (δ_{max}) with 18 cm as the standard, which is the first condition of mold base thickness, 0.258 mm was multiplied with the safety coefficient 1.5. The result was about 0.387 mm. Since the first condition 18 cm exceeded the standard range of deformation 0.20~0.25 mm, the first condition was judged as "failure" according to the expression and thus excluded from the structural simulation.

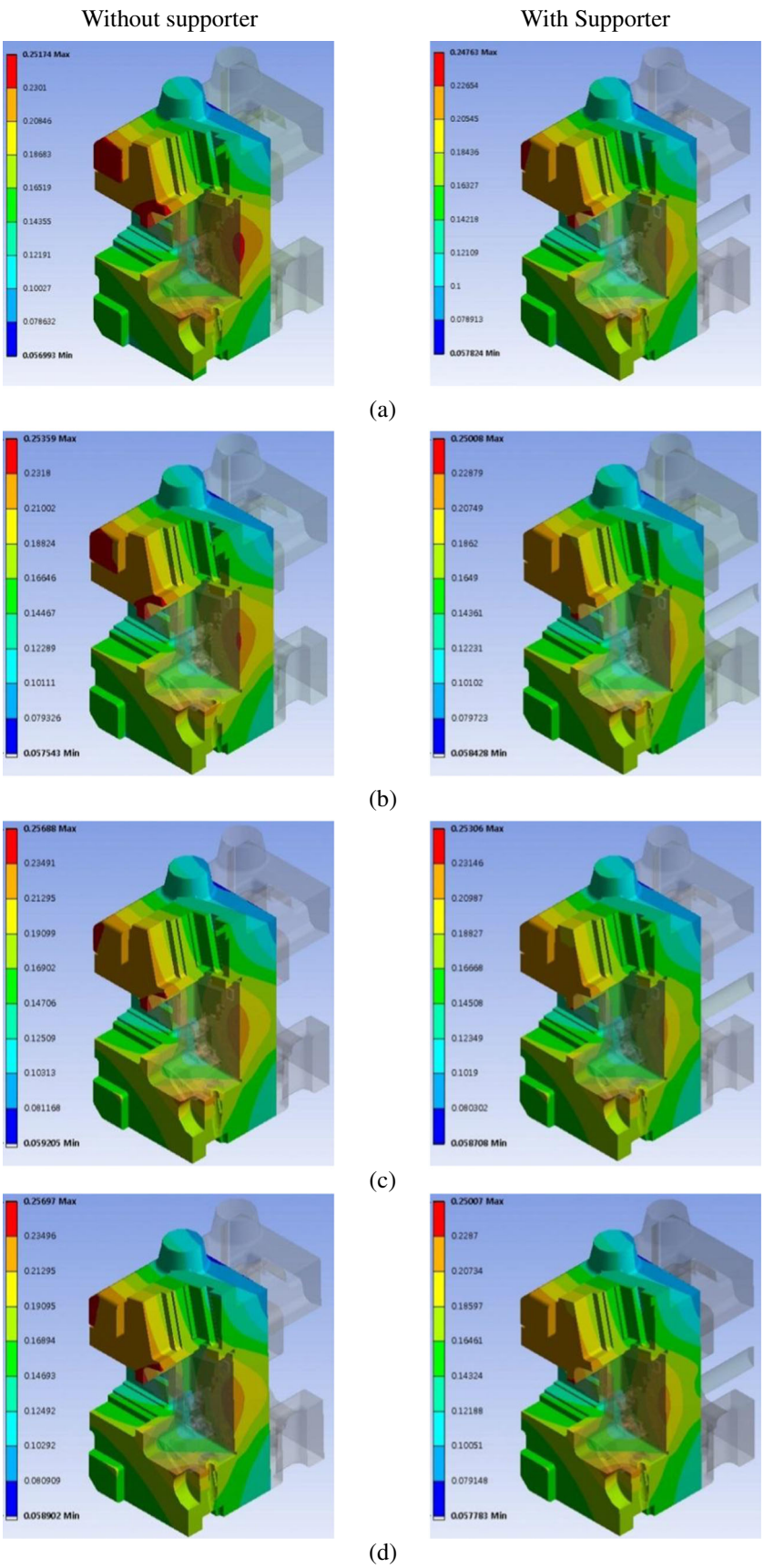

Fig. 7 Results of structural analysis for movable mold base: **a** h=20 cm, **b** h=22 cm, **c** h=24 cm, and **d** h=23 cm

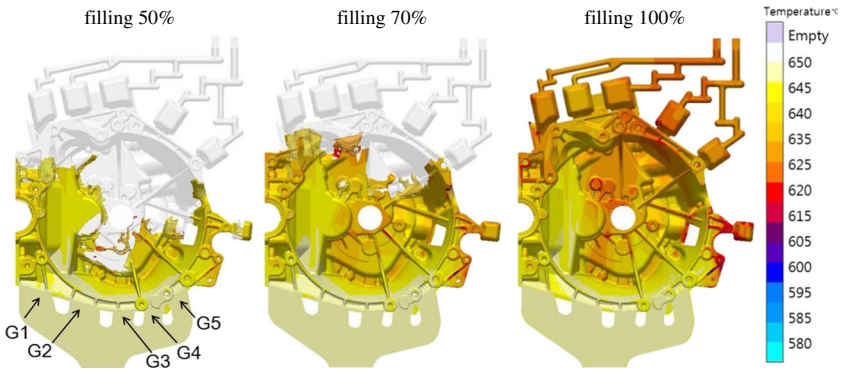

Fig. 8 Filling behavior in mold cavity

As for the second condition 20 cm, max. deflection (δ_{max}) of 0.188 mm was multiplied by the safety coefficient 1.5, and the result was about 0.282 mm. Though this value was a bit out of the standard range of deformation 0.20~0.25 mm, a structural simulation was conducted. Figure 7a shows the result of the structural simulation with the supporter both not applied and applied. As for the structure with no supporter, the deformation value was about 0.2371 mm, which indicates the deviation about 0.61 times lower than the value multiplied by the safety coefficient in the simplified expression, while in the condition with a supporter, the deformation value was 0.2178 mm, which indicates the deviation about 0.56 times lower. Hence, the second condition, 20 cm, was judged as "failure" in the structural simulation with the supporter both not applied and applied, and thus it was excluded in the step of design.

As for the third condition, 22 cm, max. deflection (δ_{max}) was 0.141 mm, which was multiplied by the safety coefficient 1.5 and the result was 0.212 mm. The result of the structural simulation is presented in Fig. 7b. As in the second case, when no supporter was applied, the value was about 0.2334 mm, 1.1 times higher than that when the expression was applied (the safety coefficient included), and when a supporter was applied, 0.2159 mm, about one time higher. Hence, the third condition too was judged as "failure" and excluded in the designing process.

As for the fourth condition, 24 cm, max. deflection (δ_{max}) was about 0.164 mm (the safety coefficient 1.5 included). Figure 7c shows the result of the structural simulation in application of the fourth condition. With no supporter, the value was 0.2248 mm, about 1.3 times more than the calculated value, and with a supporter, the value was 0.2115 mm, about 1.3 times more. In the fourth condition, the result was viewed as "good" with a supporter both not applied and applied. Hence, when the value was 24 cm, the result was satisfactory with regard to mold deformation even without a supporter.

Finally, to apply the optimal mold design, mold base thickness was modified to 23 cm, and the simplified calculation result and structural simulation result were reanalyzed. As shown in Fig. 7d, when no supporter was applied, the value was 0.2279 mm, about 1.2 times more. When a supporter was applied, the value was 0.2131 mm, about 1.1 times more. The result was judged as "good" both with and without a supporter. Hence, the final thickness was set to 23 cm, and no supporter was applied to the final mold design.

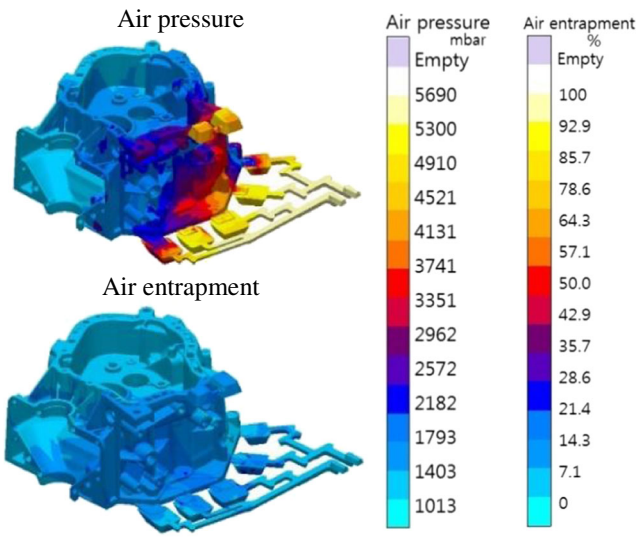

Fig. 9 Air pressure and air entrapment in mold cavity

3.2 Casting simulation

Figure 8 shows the filling behavior in reflection of temperature change. The melt flew into the mold and then filled the cavity. As for fluidity, the fluid in the middle where gate No. 2 (G2) and gate No. 3(G3) were located was slower than the average. As the charging rate increased, the filling behavior enhanced accordingly. The simulation result shows that in local spots, the melting temperature decreased under filling. Figure 9 shows the results of pressure distribution in the mold and contents of air pockets after the melt was filled in mold. The air pressure was high at the final filling area connected to the overflow. While the

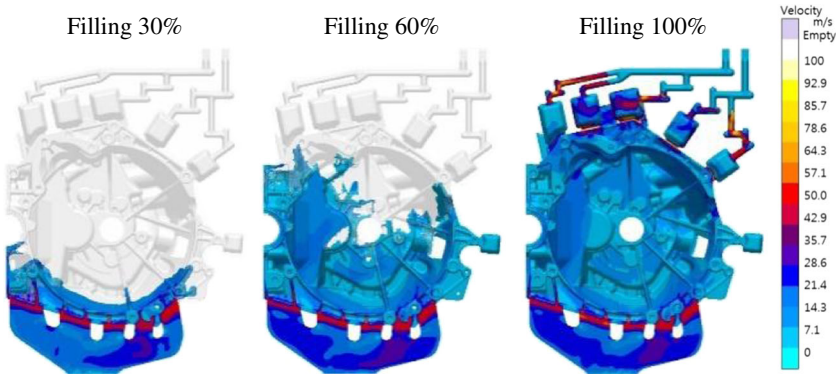

Fig. 10 Velocity distribution in mold cavity

melt was filled in the mold, the air flowing in could not get out of the vent but remained in the mold. The air entrapment experiment also shows that there was high possibility of air pocket formation in the final filling area.

Figure 10 shows the flow rates when the melt was filled in the mold. As the melt passed the runner and reached the gate, the flow rate drastically increased since the cross-sectional area of runner was smaller than that of the gate. The speed at the gate rapidly increased up to 50 m/s and then remained around 50 m/s after the location of high-speed changeover. As the plunger passed the low-speed section and entered the high-speed area, the plunger was switched to high rates when the melt passed through the narrow section of the gate, which caused the speed at the gate to drastically increase. At the final filling area, the speed increased up to 100 m/s because the sectional area at the overflow inlet suddenly decreased. At the vent runner section as well, the speed drastically increased as the melt passed through the narrow vent runner right after the relatively large area of the overflow.

Figure 11 shows the result of the solidifying behavior after the filling was completed. Solidifying behaviors were initiated at spots that were in contact with the mold or relatively thin. In contrast, at spots that were thick or too bended for heat to get out, the solidification was slow. As shown in Fig. 11, prompt solidification began at the outer part and rapidly spread to the central and left areas that were thick. At the runner and biscuit areas, which were the thickest part, solidification was quite slow. Figure 12 shows the spot where shrinkage porosity was expected. Shrinkage porosity would occur at thick spots and areas of slow solidification. In the left area that was thick and thus solidified slowly, a lot of shrinkage porosities were found.

Figure 13 shows the result of mold soldering in prediction of the spot of sticking between the mold and melt. Sticking was observed in areas of outstanding winding. To minimize the area of mold sticking, especially at areas of relatively high temperature and possible mold sticking as shown in the simulation result above, release agents and cooling spray need to be applied. Accordingly, areas of outstanding sticking were checked in the shot test and release agents and cooling spray were applied specifically to such areas.

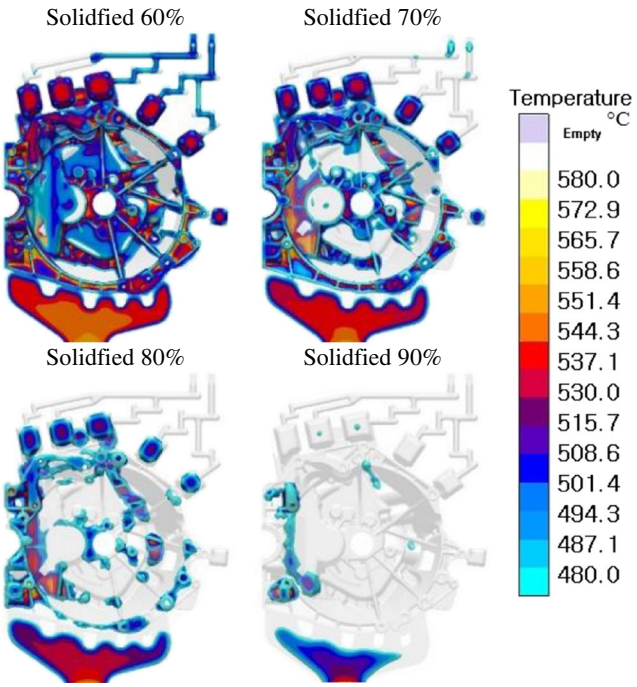

Fig. 11 Solidification behavior in mold cavity after filling finish

3.3 Castability and mechanical property

Figure 14 shows the mold temperature after pre-heating measured by means of a non-contact thermo-graphic camera. The max. temperature of the movable part was 307.7 °C and that of the other parts was 150~215 °C on average. The max temperature of the fixed mold was 312.4 °C and that of the other parts was 110~210 °C.

Figure 15 compares the temperature distribution over the solidified areas in the casting simulation with the melt temperature measurements after injection by means of a non-contact thermal infrared image camera. As shown in Fig. 15, although there was some difference in measuring time points and

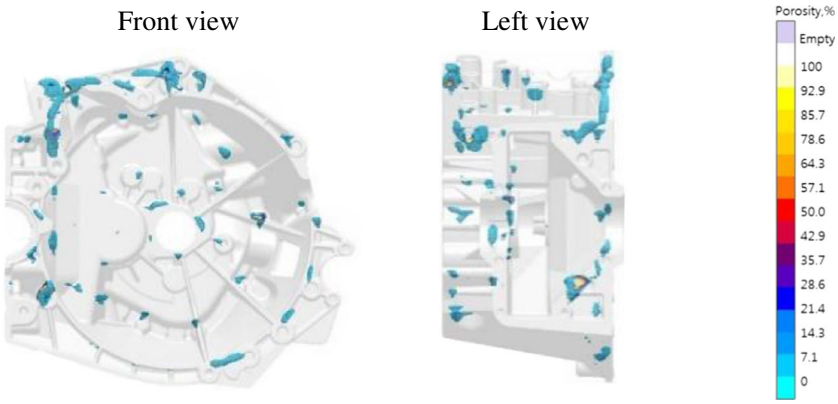

Fig. 12 Shrinkage porosity after solidification finish

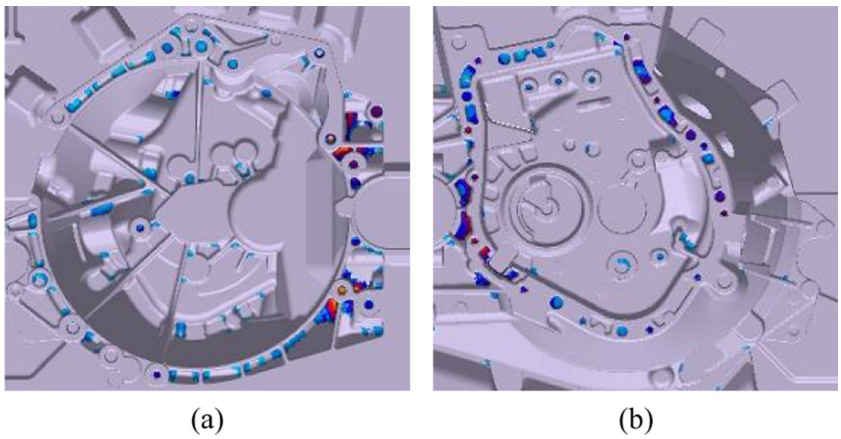

Fig. 13 Mold soldering after solidification finish: **a** fixed mold and **b** movable mold

peripheral temperature distributions, it turned out that the temperature distribution in the casting simulation was similar to the actual temperature distribution with actual melts used.

Figure 16 shows the clutch housing samples manufactured after five times shot. All of the five samples were molded with no part of incomplete formation. The sample of first shot (Fig. 16a) was filled to the chill vent section. The number of waves of the chill vent was 4 to 5, which indicates that the molten flow stopped at the point of the fourth to fifth wave formation of the chill vent. The burr around the vent insert seems to indicate the dispersion at the fixed and movable molds due to the insufficiency of clamping force.

Figure 17 shows the simulation and experiment results of the shrinkage porosity occurred during solidification. Figure 17a shows the distribution of shrinkage porosities based on the simulation result while Fig. 17b shows the section of the clutch housing sample at the same spot in the simulation. The shrinkage porosities are concentrated in the thick area at the left side, beginning from the central area. The clutch housing sample involved shrinkage porosity at a similar

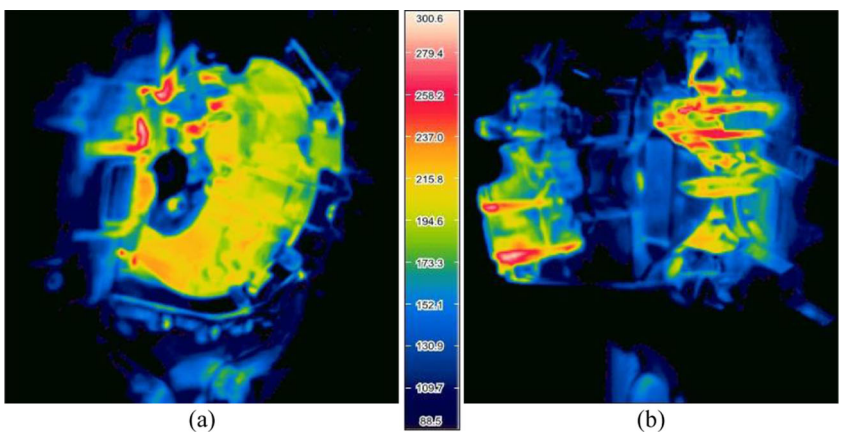

Fig. 14 Temperature distribution of molds after pre-heating measured by thermo-graphic camera: **a** fixed mold and **b** movable mold

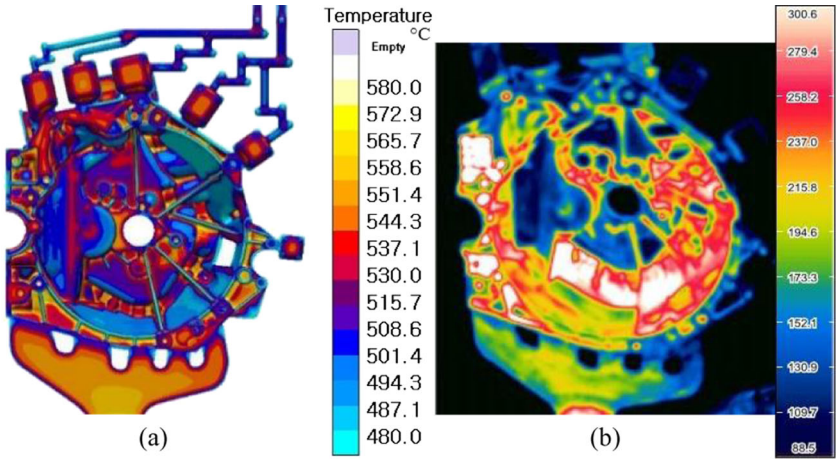

Fig. 15 Comparison of mold temperature between simulation and real shot test: **a** simulation result and **b** real shot test

but not exactly the same location. It seems that various on-site factors affected the result.

Figure 18 shows the microstructure of the clutch housing sample. Figure 18a shows the part of average thickness while Fig. 18b shows the thick part. The thick part is divided to the primary α-Al phase and eutectic phase while the part of average thickness is of one network with no division of the primary α-Al phase and eutectic phase. The latter involved a lot of needle-shaped Si in the eutectic network, which was formed upon rapid solidification at temperature lower than the eutectic temperature when the molten metal was put into the mold and reached the relatively thin part. Since the solidification was slow in the temperature range from below the eutectic temperature to room temperature (up to the quenching in water), Si particles were formed in a shape of needles. At the thick part of the product, the primary α-Al phase was formed first and then the eutectic phase. At the central part of the thick section, solidification began even in a liquid state. The primary α-Al phase was formed first and then as it was cooled down below the eutectic temperature, the eutectic phase was later formed. Si particles were not precipitated out of the eutectic network probably because water would

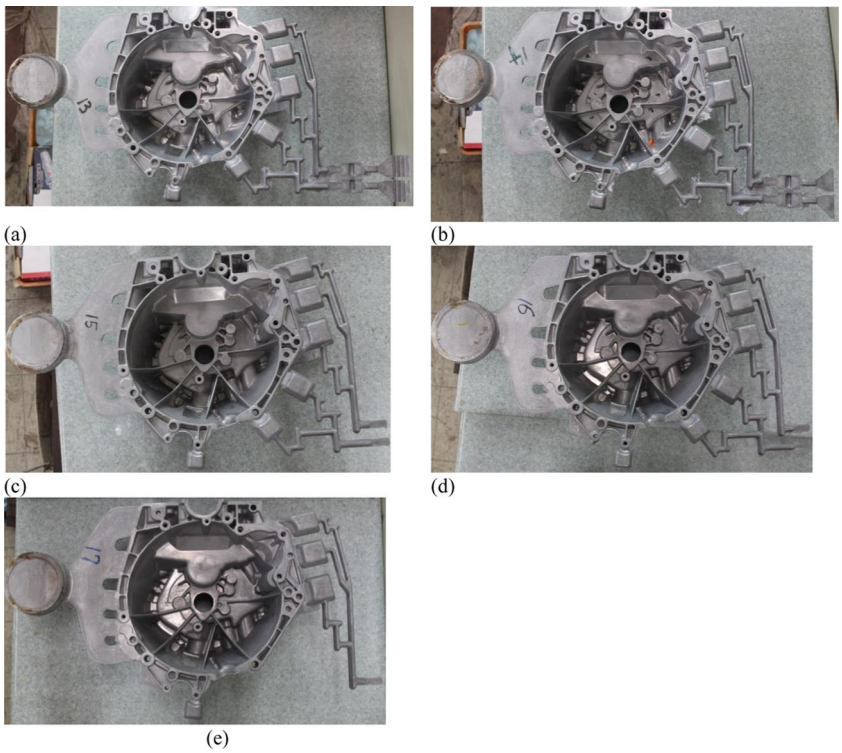

Fig. 16 Fabricated clutch housing castings: **a** first shot, **b** second shot, **c** third shot, **d** fourth shot, and **e** fifth shot

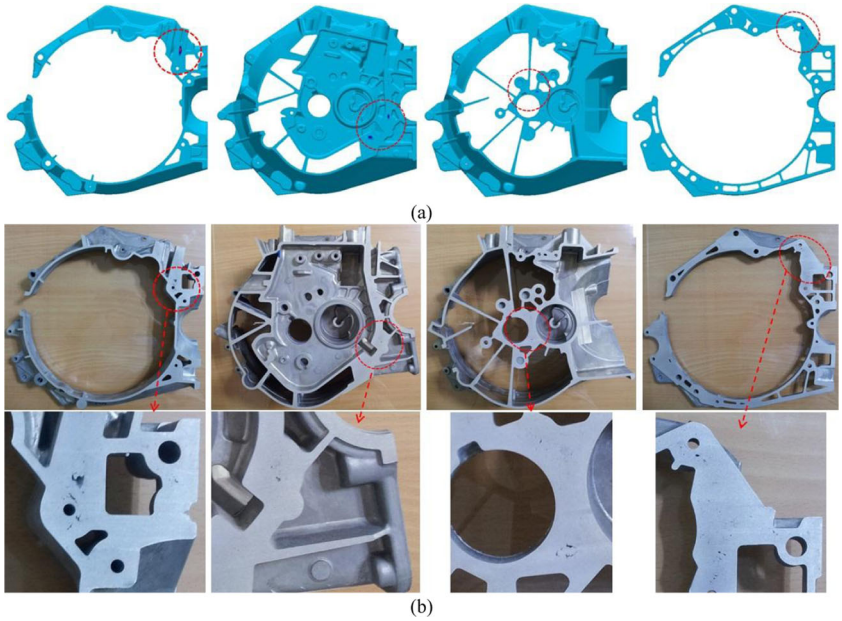

Fig. 17 Comparison of porosity distribution between simulation and real shot test

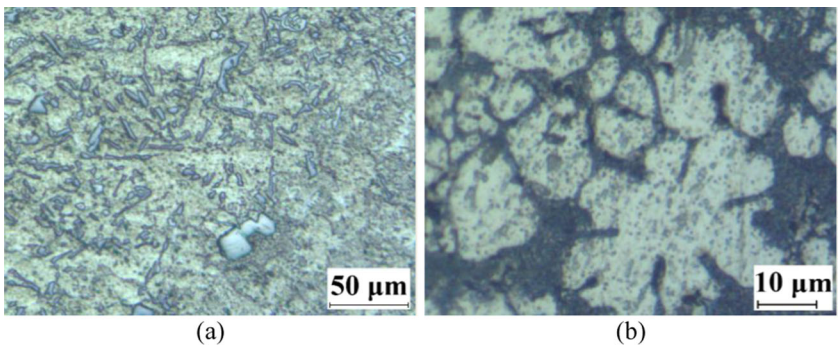

Fig. 18 Microstructures of clutch housing in different positions: **a** normal thickness and **b** thick thickness

be frozen sometime after the thick part was solidified below the eutectic temperature and thus Si particles were unable to grow. Figure 19 shows the result of measuring Vickers hardness at seven different locations of a clutch housing sample. The hardness was about 84.05 HV, and it was similar regardless of location

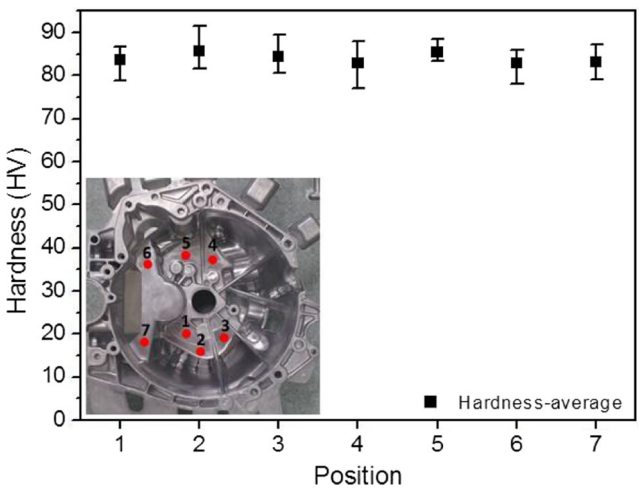

Fig. 19 Vickers hardness at different positions

4 Conclusions

This study emphasizes the importance of mold design and thus utilizes various calculation functions necessary for it.

(1) Casting devices selected significantly affect the equipment life and mold used. Furthermore, they affect the production cost and expenses for additional facilities, and most of all, the quality of final products. Thus, keen attention needs to be paid to selecting casting devices.
(2) As for the structural simulation of the mold base, the function of max. deflection (δ_{max}) for the simple beam's distributed load was utilized to design a simplified expression to calculate the result (safety coefficient). It is expected that using this simplified calculation method will reduce waste of energy and time in the thickness design of a mold base.

(3) All of the five products manufactured through the shot test, including the overflow, were perfectly formed with no incomplete formation. There was no crack or flow mark on the surface either. Vickers hardness of the products was about 84 HV regardless of location.
(4) As solidification was slow in thicker spots, shrinkage porosities were formed within the products. As for the shrinkage porosity formation in the products, the casting simulation results were somewhat different from the actual locations of shrinkage porosity formation. It seems that various factors in the actual formation site cause such difference.

Acknowledgments This work was supported by the National Research Foundation of Korea (NRF) grant funded by the Korea Government (No. 2013R1A1A2062759). This study was also supported by the National Research Foundation of Korea (KRF) grant funded by the Korea Government (MISP) through GCRC-SOP (No. 2012–0001204).

References

1. Doehler die-casting co (1916) Creating and industry. Brooklyn, New York
2. Jin CK, Bae JW, Kang CG (2014) Development of rheology vacuum low-pressure die casting with electromagnetic stirrer and vacuum system. Proc IMechE Part B J Eng Manuf 228(12):1599–1610
3. Zhang L, Wang R (2013) An intelligent system for low-pressure die-cast process parameters optimization. Int J Adv Manuf Technol 65:517–524
4. Hsu FY, Jolly MR, Campbell J (2009) A multiple-gate runner system for gravity casting. J Mater Process Technol 209:5736–5750
5. Jin CK, Kang CG (2011) Fabrication process analysis and experimental verification for aluminum bipolar plates in fuel cells by vacuum die-casting. J Power Sources 196:8241–8249
6. Kim ES, Lee KH, Moon YH (2000) A feasibility study of the partial squeeze and vacuum die casting process. J Mater Process Technol 105:42–48
7. Jin CK, Kang CG (2012) Fabrication by vacuum die casting and simulation of aluminum bipolar plates with micro-channels on both sides for proton exchange membrane (PEM) fuel cells. Int J Hydrog Energy 37:1661–1676
8. Chang QM, Chen CJ, Zhang SC, Schwam D, Wallace JF (2010) Effects of process parameters on quality of squeeze casting A356 alloy. Int J Cast Met Res 23:30–36
9. Hu BH, Tong KK, Niu XP, Pinwill I (2000) Design and optimisation of runner and gating systems for the die casting of thin-walled magnesium telecommunication parts through numerical simulation. J Mater Process Technol 105:128–133
10. Chen JH, Hwang WS, Wu CH, Lu SS (2011) Design of die casting process of top cover of automobile generator through numerical simulations and its experimental validation. Int J Cast Met Res 24:163–169
11. Jang JCH (1994) Casting plan of aluminum die castings. J Korean Foundry Soc 14(4):294–304
12. Kim ES, Lee KH (1998) High casting technology for aluminum alloy die casting (I). J Korean Foundry Soc 18(3):211–221